# THE FIELD DESCRIPTION MODEL FOR THE LHC QUADRUPOLE SUPERCONDUCTING MAGNETS*

N. Sammut#, L. Bottura, S. Sanfilippo, CERN, Geneva, Switzerland
J. Micallef, University of Malta, Malta

*Abstract*

The LHC control system requires an accurate forecast of the magnetic field and the multipole field errors to reduce the burden on the beam-based feed-back. The Field Description for the LHC (FIDEL) is the core of this forecast system and is based on the identification and physical decomposition of the effects that contribute to the total field in the magnet apertures. The effects are quantified using the data obtained from series magnetic measurements at CERN and they are consequently modelled empirically or theoretically depending on the complexity of the physical phenomena. This paper presents a description of the methodology used to model the field of the LHC magnets particularly focusing on the results obtained for the LHC main quadrupoles (MQ) and insertion region wide aperture quadrupoles (MQY).

## INTRODUCTION

The LHC requires a powerful control system to correct the field variations that result from the inherent properties of the superconducting magnets. If not corrected with high speed and precision, these field changes considerably affect the particle beam and therefore reduce the performance of the machine.

A feed-back control system based on beam measurements has limited capabilities and may not be good enough to provide the required error compensation. A system based on feed-forward control is therefore required to reduce the burden on the feed-back system by forecasting what the field (and hence tune) variations will be during particle acceleration and collision.

The Field Description for the LHC (FIDEL) is the main part of the feed-forward mechanism consisting of magnetic field model based on field mapping performed in cryogenic conditions on a sample of the magnet population. The field model has already been applied on the LHC dipole magnets [1]. In this paper, the model is applied on the LHC main quadrupole elements and is used to decompose the measured field errors and obtain the component parameters.

## COMPONENT IDENTIFICATION

A magnet can be accurately modelled by a 2d complex function that describes the integrated value of the field over the magnetic length. The complex harmonic of order $n$ can be indicated by the series expansion of the field $\boldsymbol{B}$ in the magnet aperture at a reference radius $R_{ref}$ = 17 mm using Cartesian coordinates:

$$\mathbf{B}(x,y) = \sum_{n=1}^{\infty} \boldsymbol{C}_n \left( \frac{x+iy}{R_{ref}} \right)^{n-1} \qquad (1)$$

The normalized harmonic coefficients indicated as $\mathbf{c}_n$ are used for convenience and defined as:

$$\mathbf{c}_n = b_n + ia_n = 10^4 \frac{\mathbf{C}_n}{B_m} \qquad (2)$$

expressed in units. $b_n$ and $a_n$ are the normal and skew harmonics respectively and $B_m$ indicates the main field. The main field transfer function (TF) is defined as the ratio of the main field divided by the operating current $I$. The field errors can be decomposed in the following components to give an explicit form of the model [1]:

A) *Static (DC) Components:* these are steady-state in nature and are reproducible from cycle-to-cycle provided the magnet is cycled with the same procedure, in particular the minimum and maximum excitation current irrespective of the time required for cycling and irrespective of the ramp-rate. Static components are solely dependent on the excitation current and include:

a. geometric contribution ($\mathbf{C}_n^{geometric}$).
b. DC Magnetisation Contribution ($\mathbf{C}_n^{MDC}$).
c. Saturation contribution ($\mathbf{C}_n^{saturation}$).
d. Displacement contribution ($\mathbf{C}_n^{deformation}$).
e. Residual Magnetisation Contribution ($\mathbf{C}_n^{residual}$).

B) *Dynamic (AC) Components:* These components are both current and time dependent and are not reproducible from cycle-to-cycle. They include:

a. Decay ($\mathbf{C}_n^{decay}$).
b. Snap-back ($\mathbf{C}_n^{snap-back}$).
c. Coupling-Currents ($\mathbf{C}_n^{MAC}$).

The field model can be decomposed in this way because each component is considered to be mutually independent from the others. This is justified because each of the components has a distinct and independent physical origin. The field model can therefore be expressed by a sum of the components:

$$\mathbf{C}_n = \mathbf{C}_n^{geometric} + \mathbf{C}_n^{MDC} + \mathbf{C}_n^{saturation} + \mathbf{C}_n^{deformation} + \mathbf{C}_n^{residual} + \mathbf{C}_n^{decay} + \mathbf{C}_n^{snap-back} + \mathbf{C}_n^{MAC} \qquad (3)$$

## MODEL FORMULATION

Based on the component identification presented above and on the mathematical formulation presented in [1], the transfer function in the static domain can be fitted with the following non-linear equation with the parameter definitions described in Table 1:

$$TF^{static}_{up/down} = \gamma_m \pm \mu_m \left( \frac{I_{inj}}{I} \right) \left( \frac{I}{I_{inj}} \right)^{p_m} \left( \frac{I_c - I}{I_c - I_{inj}} \right)^{q_m} \left( \frac{T_{co}^{1.7} - T^{1.7}}{T_{co}^{1.7} - T_{meas}^{1.7}} \right)^{m_m} + \sum_{i=1}^{N} \sigma_m^i \Sigma \left( \frac{1}{\pi} \mathrm{atan} \left( S_m^i \left( \frac{I - I_{0,m}^i}{I_{nom}} \right) \right) + \frac{1}{2} \right) + \rho_m \left( \frac{I_{inj}}{I} \right)^{\gamma_m} \qquad (4)$$

where the first term describes the geometric contribution, and the second term describes the magnetisation

* Work supported by CERN; #nicholas.sammut@cern.ch

contribution (positive for ramp-up and negative for ramp-down). The third term empirically describes both the saturation and displacement contribution and the fourth term describes the residual magnetisation contribution. Even though the coupling currents contribution is expected to be large [2], no data is available for modeling to date. Therefore this component is omitted from Eq. 4.

In the dynamic domain, the decay can be modelled with the following equation [3]:

$$TF^{decay} = \delta_m \left[ d_m \left( 1 - e^{-\frac{t-t_{inj}}{\tau_m}} \right) + (1-d_m) \left( 1 - e^{-\frac{t-t_{inj}}{9\tau_m}} \right) \right] \quad (5)$$

which is justified as a result of the current redistribution in the superconducting cables. The definitions of the parameters are shown in Table 1. Unfortunately, no reliable snap-back data is available for the LHC quadrupoles to date.

Table 1: Definitions of parameters in model formulation.

| Symbol | Meaning | TF | $b_6$ |
|---|---|---|---|
| $\gamma$ | geometric field error | Tm/kA | (units) |
| $\mu$ | DC magnetization strength | (units) | (units) |
| $p$ | DC magnetization pinning exponent | (-) | (-) |
| $q$ | DC magnetization pinning exponent | (-) | (-) |
| $m$ | DC magnetization pinning exponent | (-) | (-) |
| $T$ | temperature | (K) | (K) |
| $T_{co}$ | critical temperature | (K) | (K) |
| $T_{meas}$ | temperature during measurement | (K) | (K) |
| $\sigma$ | iron saturation strength | (units) | (units) |
| $I_0$ | iron saturation current | (A) | (A) |
| $S$ | iron saturation current range | (-) | (-) |
| $N$ | number of smooth step functions | (-) | (-) |
| $\rho$ | residual magnetization strength | (units) | (units) |
| $r$ | residual magnetization exponent | (-) | (-) |
| $\delta$ | decay strength | (units) | (units) |
| $d$ | fast decay normalized amplitude | (-) | (-) |
| $\tau$ | decay time constant | (s) | (s) |
| $\Delta I$ | snap-back current constant | (A) | (A) |
| $I$ | current | (A) | (A) |
| $t$ | time | (s) | (s) |
| $I_{inj}$ | current at injection | (A) | (A) |
| $I_{nom}$ | nominal current | (A) | (A) |
| $I_c$ | critical current | (A) | (A) |
| $t_{inj}$ | time at beginning of injection | (s) | (s) |

## RESULTS FOR THE MAIN QUADRUPOLE (MQ)

The modeling procedure described above was implemented on a sample of the main quadrupoles [4]. The measurements were performed on 61 apertures using rotating coils and a single stretch wire system [5]. The data collected represents a sample of 8% of the magnet population. An average of the data was computed and the TF was obtained in units by referring it to the geometric value at 5000 A. Eq. 4 was then fitted to the average data.

Figure 1 shows the FIDEL static model for the MQ during ramp-up. The fit is comparable to the measurement reproducibility with a maximum error of 0.36 units for the main field and 0.023 units for $b_6$ in the operating range (760 A to 11850 A).

Figure 2 shows the MQ decay model (Eq. 5) based on 27 aperture measurements at injection current.

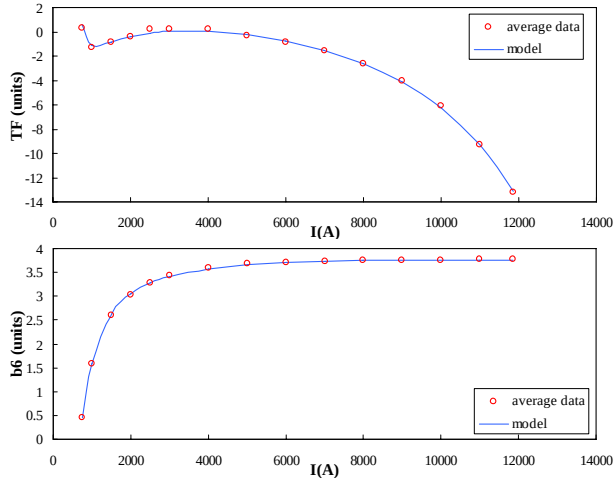


Figure 1: MQ measurements and the FIDEL model fit for (top) the main field and (bottom) the $b_6$ harmonic. For the TF, the geometric shift is removed and set to 0.

The decay curves were shifted to start from 0 on the y-axis before computing the average. This was done to decouple the decay from the current-dependent hysteresis loop. The maximum error is very small (0.1 units for the main field and 0.01 units for $b_6$) and is comparable to the measurement reproducibility in both cases. The values of the parameters are shown in Table 2. Note that even though the $b_6$ decay is significant and can be modelled well with FIDEL, this harmonic cannot be corrected in the machine since there are no correctors for it. However, this data is may be useful to eventually infer the $b_6$ snapback behaviour to the main quadrupole field.

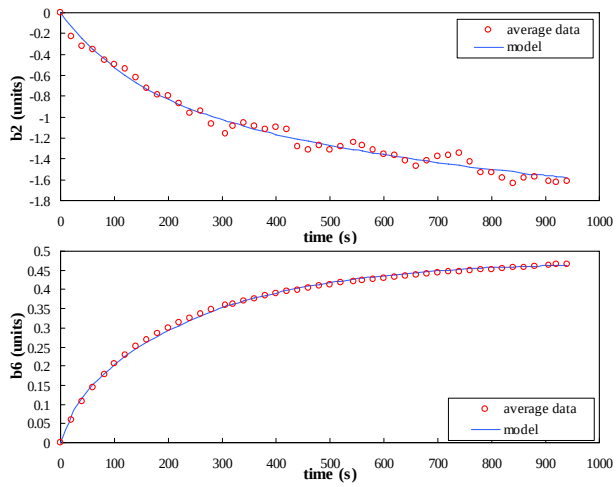


Figure 2: decay fit for the MQ for the main field and $b_6$.

## RESULTS FOR THE INSERTION REGION WIDE APERTURE QUADRUPOLE (MQY)

The FIDEL static model was also applied to the MQYs [6]. These measurements were performed using twin rotating coils. 6 apertures were measured in total representing a sample of 12% of the magnet population. The average of these measurements was computed and a fit in the static domain was performed using Eq. 4. The TF was converted into units for convenience by using the geometric value (2000 A) as reference.

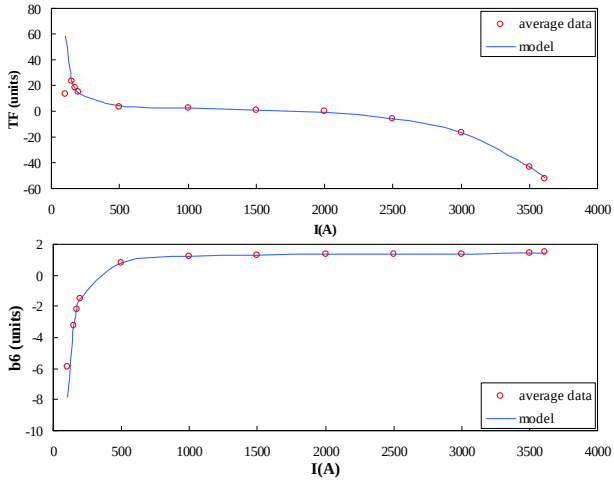


Figure 3: MQY measurements and the FIDEL model fit for (top) the main field and (bottom) the $b_6$ harmonic. For the TF, the geometric shift is removed and set to 0.

Figure 3 shows the FIDEL model for the MQY during ramp-up. The fit works very well in the range of 150 A to 3610 A since it only has a maximum error of 0.96 units for the main field and 0.043 units for the $b_6$ harmonic. For excitation values below 150A, the superconducting filaments are not fully penetrated and therefore the model does not hold well enough. This is shown as the first point in both graphs of Figure 3.

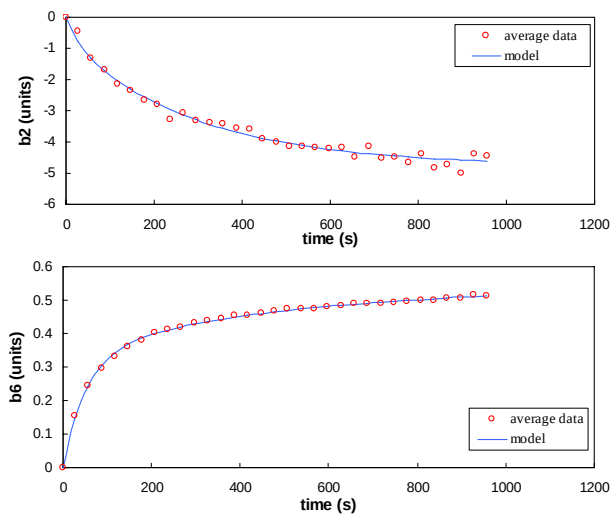


Figure 4: the decay fit for the MQY for (top) the main field (bottom) $b_6$.

Figure 4 shows the decay model (Eq. 5) based on 4 aperture measurements. The decay curves are arbitrarily shifted to start from 0 on the y-axis as was done in the case of the MQs. The maximum error of the fit is very small (0.42 units for the main field and 0.004 units for $b_6$) and is within measurement reproducibility in both cases. The values of the parameters are listed in Table 2.

## CONCLUSION

It has been shown that the FIDEL model previously used to forecast the magnetic field of LHC dipoles is robust enough to adapt to different magnet types. In this case, it was employed on the LHC focusing elements: the MQs and MQYs and has performed very well in the major hysteresis loop with maximum errors comparable to the measurement reproducibility. However, for low fields where the superconducting filaments are not fully penetrated, more measurements and further development on the model are required.

Table 2: Parameters for MQ & MQY (units as in Table 1)

| Coeft | MQ TF | MQ $b_6$ | MQY TF | MQY $b_6$ |
|---|---|---|---|---|
| $\gamma$ | 0.99275 | 3.852 | 2.5887 | 1.436 |
| $\mu$ | -3.000 | -3.258 | 12.741 | -3.557 |
| $p$ | 0.000 | -0.455 | 0.000 | -0.691 |
| $q$ | 2.000 | 0.494 | 2.000 | -0.352 |
| $m$ | 2.000 | 2.000 | 2.000 | 2.000 |
| $T$ | 1.89 | 1.89 | 1.89 | 1.89 |
| $T_{co}$ | 9.5 | 9.5 | 9.5 | 9.5 |
| $T_{meas}$ | 1.89 | 1.89 | 1.89 | 1.89 |
| $\sigma 1$ | -1420.4 | -0.065 | -182.5 | 0.051 |
| $I_0 1$ | 15703.7 | 8096.2 | 3761.8 | 3000.2 |
| $S1$ | 64.186 | 9.656 | 5.596 | 55444.6 |
| $\sigma 2$ | 8.643 | - | 34.191 | - |
| $I_0 2$ | -14.572 | - | 1683.8 | - |
| $S2$ | 4.405 | - | 1.780 | - |
| $N$ | 2 | 1 | 2 | 1 |
| $\rho$ | 3.595 | -0.144 | 5.000 | -0.037 |
| $r$ | 4.797 | 1.365 | 3.475 | 0.566 |
| $\delta$ | -1.618 | 0.466 | -4.640 | 0.514 |
| $d$ | 0.353 | 0.167 | 0.154 | 0.622 |
| $\tau$ | 138.49 | 28.386 | 32.873 | 53.690 |
| $I$ | 760 <$I$ $I$<11850 | 760 <$I$ $I$<11850 | 150<$I$ $I$<3610 | 150<$I$ $I$<3610 |
| $I_{inj}$ | 760 | 760 | 176 | 176 |
| $I_{nom}$ | 11850 | 11850 | 3610 | 3610 |
| $I_c$ | 15000 | 15000 | 15000 | 15000 |

## REFERENCES

[1] N. Sammut, L. Bottura, J. Micallef "Mathematical Formulation to Predict the Harmonics of the Superconducting Large Hadron Collider", Phys. Rev. ST Accel. Beams, 9, 012402, January 2006.

[2] O. Brüning, "Accumulation and Ramping in the LHC", LHC Project Note 218, CERN, Geneva, Feb 2000.

[3] N. Sammut, L. Bottura, P. Bauer, T. Pieloni, J. Micallef, "Three Scaling Laws to Predict the Dynamic field Changes of the Superconducting LHC Dipole Magnets", *To be published*.

[4] M. Peyrot, J.M. Rifflet, F. Simon, T. Tortschanoff, P. Vedrine, "Construction of the New Prototype of the Main Quadrupole Cold Masses for the Arc Short Straight Sections of LHC", IEEE Trans. Appl. Sup. 10 (2000) No.1, pp. 170-173.

[5] S. Sanfilippo, P. Hagen, J.P. Koutchouk, M. Giovanozzi, T. Risselada, "Transfer Function of the Quadrupoles and β-Beating", LHC Project Workshop, Chamonix XV, Divonne, Jan 2006.

[6] R. Ostojic, "Superconducting Magnets for LHC Insertions", IEEE Trans. Appl. Sup. 14(2004) No.2, pp. 181-186.